Non-spherical gold nanoparticles trapped in optical tweezers: shape matters

Oto Brzobohatý*, Martin Šiler, Jan Trojek, Lukáš Chvátal, Vítězslav Karásek, and Pavel Zemánek

Institute of Scientific Instruments of the ASCR, v.v.i. Královopolská 147, 612 64 Brno, Czech Republic

*otobrzo@isibrno.cz

Abstract: We present the results of a theoretical analysis focused on three-dimensional optical trapping of non-spherical gold nanoparticles using a tightly focused laser beam (i.e. optical tweezers). We investigate how the wavelength of the trapping beam enhances trapping stiffness and determines the stable orientation of nonspherical nanoparticles in the optical trap which reveals the optimal trapping wavelength. We consider nanoparticles with diameters being between 20 nm and 254 nm illuminated by a highly focused laser beam at wavelength 1064 nm and compare our results based on the coupled-dipole method with published theoretical and experimental data. We demonstrate that by considering the non-spherical morphology of the nanoparticle we can explain the experimentally observed three-dimensional trapping of plasmonic nanoparticles with size higher than 170 nm. These results will contribute to a better understanding of the trapping and alignment of real metal nanoparticles in optical tweezers and their applications as optically controllable nanosources of heat or probes of weak forces and torques.

OCIS codes: (020.7010) Laser trapping; (170.4520) Optical confinement and manipulation; (350.4855) Optical tweezers or optical manipulation.

References and links

1. K. C. Neuman and S. M. Block, “Optical trapping,” Rev. Sci. Instr. **75**, 2787–2809 (2004).
2. R. W. Bowman and M. J. Padgett, “Optical trapping and binding,” Rep. Prog. Phys. **76**, 026401 (2013).
3. W. J. Greenleaf, M. T. Woodside, and S. M. Block, “High-resolution, single-molecule measurements of biomolecular motion,” Annu. Rev. Biophys. Biomol. Struct. **36**, 171–190 (2007).
4. J. R. Moffitt, Y. R. Chemla, S. B. Smith, and C. Bustamante, “Recent advances in optical tweezers,” Ann. Rev. Biochem. **77**, 205–228 (2008).
5. D. Ou-Yang and M.-T. Wei, “Complex fluids: Probing mechanical properties of biological systems with optical tweezers,” Annu. Rev. Phys. Chem. **61**, 421–440 (2010).
6. A. Jonáš and P. Zemánek, “Light at work: The use of optical forces for particle manipulation, sorting, and analysis.” Electophoresis **29**, 4813–4851 (2008).
7. T. Čižmár, M. Šiler, and P. Zemánek, “An optical nanotrap array movable over a milimetre range,” Appl. Phys. B **84**, 197–203 (2006).
8. T. Čižmár, V. Garcés-Chávez, K. Dholakia, and P. Zemánek, “Optical conveyor belt for delivery of submicron objects,” Appl. Phys. Lett. **86**, 174101 (2005).
9. O. Brzobohatý, V. Karásek, M. Šiler, L. Chvátal, T. Čizmár, and P. Zemánek, “Experimental demonstration of optical transport, sorting and self-arrangement using a ‘tractor beam’,” Nature Photon. **7**, 123–127 (2013).
10. T. Čižmár, O. Brzobohatý, K. Dholakia, and P. Zemánek, “The holographic optical micro-manipulation system based on counter-propagating beams,” Laser Phys. Lett. **8**, 50–56 (2011).

11. K. Ladavac and D. G. Grier, "Colloidal hydrodynamic coupling in concentric optical vortices," Europhys. Lett. **70**, 548–554 (2005).
12. M. Reichert and H. Stark, "Circling particles and drafting in optical vortices," J. Phys.: Condens. Matter **16**, S4085–S4094 (2004).
13. K. Ladavac and D. Grier, "Microoptomechanical pumps assembled and driven by holographic optical vortex arrays," Opt. Express **12**, 1144–1149 (2004).
14. V. Karásek, T. Čižmár, O. Brzobohatý, P. Zemánek, V. Garcés-Chávez, and K. Dholakia, "Long-range one-dimensional longitudinal optical binding," Phys. Rev. Lett. **101**, 143601 (2008).
15. O. Brzobohatý, V. Karásek, T. Čižmár, and P. Zemánek, "Dynamic size tuning of multidimensional optically bound matter," Appl. Phys. Lett. **99**, 101105 (2011).
16. O. Brzobohatý, V. Karásek, M. Šiler, J. Trojek, and P. Zemánek, "Static and dynamic behavior of two optically bound microparticles in a standing wave," Opt. Express **19**, 19613–19626 (2011).
17. N. K. Metzger, E. M. Wright, W. Sibbett, and K. Dholakia, "Visualization of optical binding of microparticles using a femtosecond fiber optical trap," Opt. Express **14**, 3677–3687 (2006).
18. N. K. Metzger, R. F. Marchington, M. Mazilu, R. L. Smith, K. Dholakia, and E. M. Wright, "Measurement of the restoring forces acting on two optically bound particles from normal mode correlations," Phys. Rev. Lett. **98**, 068102 (2007).
19. K. Dholakia and P. Zemánek, "Gripped by light: Optical binding," Rev. Mod. Phys. **82**, 1767–1791 (2010).
20. T. N. Buican, M. J. Smyth, H. A. Crissman, G. C. Salzman, C. C. Stewart, and J. Martin, "Automated single-cell manipulation and sorting by light trapping," Appl. Opt. **26**, 5311–5316 (1987).
21. M. P. MacDonald, G. C. Spalding, and K. Dholakia, "Microfluidic sorting in an optical lattice," Nature **426**, 421–424 (2003).
22. T. M. Grzegorczyk, B. A. Kemp, and J. A. Kong, "Passive guiding and sorting of small particles with optical binding forces," Opt. Lett. **31**, 3378–3380 (2006).
23. I. Ricárdez-Vargas, P. Rodríguez-Montero, R. Ramos-García, and K. Volke-Sepúlveda, "Modulated optical sieve for sorting of polydisperse microparticles," Appl. Phys. Lett. **88**, 121116:1–3 (2006).
24. T. Čižmár, M. Šiler, M. Šerý, P. Zemánek, V. Garcés-Chávez, and K. Dholakia, "Optical sorting and detection of sub-micron objects in a motional standing wave," Phys. Rev. B **74**, 035105:1–6 (2006).
25. P. Jákl, V. Arzola, M. Šiler, L. Chvátal, K. Volke-Sepúlveda, and P. Zemánek, "Optical sorting of nonspherical and living microobjects in moving interference structures," Opt. Express **22**, 29746–29760 (2014).
26. A. Maslov and V. Astratov, "Microspherical photonics: Sorting resonant photonic atoms by using light," Appl. Phys. Lett. **105**, 121113 (2014).
27. S. H. Simpson, "Inhomogeneous and anisotropic particles in optical traps: Physical behaviour and applications," J. Quant. Spectrosc. Radiat. Transf. **146**, 81–99 (2014).
28. S. H. Simpson and S. Hanna, "Optical trapping of spheroidal particles in Gaussian beams," J. Opt. Soc. Am. A **24**, 430 (2007).
29. T. A. Nieminen, V. L. Y. Loke, A. B. Stilgoe, G. Knöner, A. M. Brańczyk, N. R. Heckenberg, and H. Rubinsztein-Dunlop, "Optical tweezers computational toolbox," J. Opt. A: Pure Appl. Opt. **9**, S196–S203 (2007).
30. F. Xu, K. Ren, G. Gouesbet, X. Cai, and G. Gréhan, "Theoretical prediction of radiation pressure force exerted on a spheroid by an arbitrarily shaped beam," Phys. Rev. E **75**, 026613 (2007).
31. F. Xu, J. A. Lock, G. Gouesbet, and C. Tropea, "Radiation torque exerted on a spheroid: Analytical solution," Phys. Rev. A **78**, 013843 (2008).
32. S. H. Simpson and S. Hanna, "Optical angular momentum transfer by Laguerre-Gaussian beams," J. Opt. Soc. Am. A **26**, 625–638 (2009).
33. H. Sosa-Martínez and J. C. Gutiérrez-Vega, "Optical forces on a Mie spheroidal particle arbitrarily oriented in a counterpropagating trap," J. Opt. Soc. Am. B **26**, 2109–2116 (2009).
34. A. Hinojosa-Alvarado and J. C. Gutiérrez-Vega, "Geometrical optics calculation of forces and torques produced by a ringed beam on a prolate spheroid," J. Opt. Soc. Am. B **27**, 1651–1658 (2010).
35. S. H. Simpson and S. Hanna, "Computational study of the optical trapping of ellipsoidal particles," Phys. Rev. A **84**, 053808 (2011).
36. S. H. Simpson and S. Hanna, "Application of the discrete dipole approximation to optical trapping calculations of inhomogeneous and anisotropic particles," Opt. Express **19**, 16526–16541 (2011).
37. J. Trojek, L. Chvátal, and P. Zemánek, "Optical alignment and confinement of an ellipsoidal nanorod in optical tweezers: a theoretical study," J. Opt. Soc. Am. A **29**, 1224–1236 (2012).
38. K. Bonin, B. Kourmanov, and T. Walker, "Light torque nanocontrol, nanomotors and nanorockers," Opt. Express **10**, 984–989 (2002).
39. Z. Cheng, P. Chaikin, and T. Mason, "Light streak tracking of optically trapped thin microdisks," Phys. Rev. Lett. **89**, 108303 (2002).
40. P. Galajda and P. Ormos, "Orientation of flat particles in optical tweezers by linearly polarized light," Opt. Express **11**, 446–451 (2003).
41. B. M. Mihiretie, P. Snabre, J. C. Loudet, and B. Pouligny, "Radiation pressure makes ellipsoidal particles tumble," Europhys. Lett. **100**, 48005 (2012).

#232067 - $15.00 USD Received 8 Jan 2015; revised 27 Feb 2015; accepted 28 Feb 2015; published 23 Mar 2015

42. A. Arzola, P. Jákl, L. Chvátal, and P. Zemánek, “Rotation, oscillation and hydrodynamic synchronization of optically trapped oblate spheroidal microparticles,” Opt. Express **22**, 16207–16221 (2014).
43. A. Bishop, T. Nieminen, N. Heckenberg, and H. Rubinsztein-Dunlop, “Optical application and measurement of torque on microparticles of isotropic nonabsorbing material,” Phys. Rev. A **68**, 033802 (2003).
44. L. Oroszi, P. Galajda, H. Kirei, S. Bottka, and P. Ormos, “Direct measurement of torque in an optical trap and its application to double-strand DNA,” Phys. Rev. Lett. **97**, 058301 (2006).
45. B. Gutierrez-Medina, J. O. Andreasson, W. J. Greenleaf, A. LaPorta, and S. M. Block, “An optical apparatus for rotation and trapping,” Methods Enzymol. **475**, 377–404 (2010).
46. D. Phillips, M. Padgett, S. Hanna, Y.-L. Ho, D. Carberry, M. Miles, and S. Simpson, “Shape-induced force fields in optical trapping,” Nature Photon. **8**, 400–405 (2014).
47. K. Svoboda and S. M. Block, “Optical trapping of metallic Rayleigh particles,” Opt. Lett. **19**, 930–932 (1994).
48. M. Pelton, M. Liu, H. Kim, G. Smith, P. Guyot-Sionnest, and N. Scherer, “Optical trapping and alignment of single gold nanorods by using plasmon resonances,” Opt. Lett. **31**, 2075–2077 (2006).
49. J. K. C. Toussaint, M. Liu, M. Pelton, J. Pesic, M. J. Guffey, P. Guyot-Sionnest, and N. F. Scherer, “Plasmon resonance-based optical trapping of single and multiple Au nanoparticles,” Opt. Express **15**, 12017–12029 (2007).
50. R. Saija, P. Denti, F. Borghese, O. M. Maragò, and M. A. Iatì, “Optical trapping calculations for metal nanoparticles. comparison with experimental data for au and ag spheres.” Opt. Express **17**, 10231–10241 (2009).
51. P. M. Hansen, V. K. Bhatia, N. Harrit, and L. Oddershede, “Expanding the optical trapping range of gold nanoparticles,” Nano Lett. **5**, 1937–1942 (2005).
52. M. A. Yurkin and A. G. Hoekstra, “The discrete-dipole-approximation code adda: Capabilities and known limitations,” J. Quant. Spectrosc. Radiat. Transf. **112**, 2234–2247 (2011).
53. B. J. Wiley, S. H. Im, Z.-Y. Li, J. McLellan, A. Siekkinen, and Y. Xia, “Maneuvering the surface plasmon resonance of silver nanostructures through shape-controlled synthesis,” J. Phys. Chem. B **110**, 15666–15675 (2006).
54. X. Lu, M. Rycenga, S. E. Skrabalak, B. Wiley, and Y. Xia, “Chemical synthesis of novel plasmonic nanoparticles,” Annu. Rev. Phys. Chem. **60**, 167–192 (2009).
55. O. Brzobohatý, M. Šiler, J. Trojek, L. Chvátal, V. Karásek, A. Paták, Z. Pokorná, F. Mika, and P. Zemánek, “Three-dimensional optical trapping of a plasmonic nanoparticle using low numerical aperture optical tweezers,” Sci. Rep. **5**, 8106 (2014).
56. B. Richards and E. Wolf, “Electromagnetic diffraction in optical systems. 2. Structure of the image field in an aplanatic system,” Proc. Royal Soc. London A **253**, 358–379 (1959).
57. J. J. Stamnes, *Waves in Focal Regions.* (Taylor & Francis Group, Bristol, 1986).
58. O. Brzobohatý, M. Šiler, J. Ježek, P. Jákl, and P. Zemánek, “Optical manipulation of aerosol droplets using a holographic dual and single beam trap,” Opt. Lett. **38**, 4601–4604 (2013).
59. A. Kyrsting, P. M. Bendix, and L. B. Oddershede, “Mapping 3D focal intensity exposes the stable trapping positions of single nanoparticles,” Nano Lett. **13**, 31–35 (2013).
60. J. P. B. Schaub, D. R. Alexander, and S. A., “Theoretical determination of net radiation force and torque for a spherical particle illuminated by a focused laser beam,” J. Appl. Phys. **66**, 4594–4602 (1989).
61. G. Gouesbet and G. Gréhan, *Generalized Lorenz-Mie Theories* (Springer, 2011).
62. B. T. Draine and P. J. Flatau, “Discrete-dipole approximation for scattering calculations,” J. Opt. Soc. Am. A **11**, 1491–1499 (1994).
63. A. G. Hoekstra, M. Frijlink, L. B. F. M. Waters, and P. M. A. Sloot, “Radiation forces in the discrete-dipole approximation,” J. Opt. Soc. Am. A **18**, 1944–1953 (2001).
64. V. Karásek, O. Brzobohatý, and P. Zemánek, “Longitudinal optical binding of several spherical particles studied by the coupled dipole method,” J. Opt. A: Pure Appl. Opt. **11**, 034009 (2009).
65. E. Messina, E. Cavallaro, A. Cacciola, M. A. Iatì, P. G. Gucciardi, F. Borghese, P. Denti, R. Saija, G. Compagnini, M. Meneghetti, V. Amendola, and O. M. Maragò, “Plasmon-enhanced optical trapping of gold nanoaggregates with selected optical properties,” ACS Nano **5**, 905–913 (2011).
66. V. Myroshnychenko, J. Nelayah, G. Adamo, N. Geuquet, J. Rodriguez-Fernandez, I. Pastoriza-Santos, K. F. MacDonald, L. Henrard, L. M. Liz-Marzan, N. I. Zheludev, M. Kociak, and F. Javier Garcia de Abajo, “Plasmon spectroscopy and imaging of individual gold nanodecahedra: A combined optical microscopy, cathodoluminescence, and electron energy-loss spectroscopy study,” Nano Lett. **12**, 4172–4180 (2012).
67. P. Das and T. K. Chini, “Spectroscopy and imaging of plasmonic modes over a single decahedron gold nanoparticle: A combined experimental and numerical study,” J. Phys. Chem. C **116**, 25969–25976 (2012).
68. J. Rodriguez-Fernandez, C. Novo, V. Myroshnychenko, A. M. Funston, A. Sanchez-Iglesias, I. Pastoriza-Santos, J. Perez-Juste, F. J. Garcia de Abajo, L. M. Liz-Marzan, and P. Mulvaney, “Spectroscopy, imaging, and modeling of individual gold decahedra,” J. Phys. Chem. C **113**, 18623–18631 (2009).
69. R. Agayan, F. Gittes, R. Kopelman, and C. Schmidt, “Optical trapping near resonance absorption,” Appl. Opt. **41**, 2318–2327 (2002).
70. J. R. Arias-González and M. Nieto-Vesperinas, “Optical forces on small particles: attractive and repulsive nature and plasmon-resonance conditions,” J. Opt. Soc. Am. A **20**, 1201 (2003).

71. M. Dienerowitz, M. Mazilu, P. J. Reece, T. F. Krauss, and K. Dholakia, "Optical vortex trap for resonant confinement of metal nanoparticles," Opt. Express **16**, 4991–4999 (2008).
72. E. Palik and G. Ghosh, *Handbook of Optical Constants of Solids* (Academic Press, 1998).

1. Introduction

The behavior of spherical objects in focused or structured trapping beams has been extensively investigated from the theoretical and experimental point of view during the last 3 decades [1–6]. The primary effort has been focused on dielectric spheres and many interesting observations and applications have been reported: e.g. optical delivery from micrometer up to millimeter distances [7–9] (optical conveyor belt, tractor beams), particles orbiting in optical vortex beams [10–12], fluid-flow convection due to moving or rotating spheres [13] (optical motors and pumps), optical self-arrangement of many particles due to their mutual interaction through the scattered light [2, 14–19] (optical binding), separation of spheres of different diameters or materials [6, 20–26] (optical sorting), measurement of tiny forces using optically trapped probes [3–5](optical pikotenzometers). With the advance of computational power more complex shapes started to be investigated theoretically [27–37] and experimentally [38–46]. In addition to optical forces and consequent particles trapping, optical torques and particle rotation have to be investigated which leads to another level of complexity.

With the boom of plasmonics more attention has been focused on optical manipulation with metal nanoparticles (NPs) even though the pioneering experiments of Svoboda and Block were reported a relatively long time ago [47]. In contrast to dielectric particles, metal NPs change their optical properties significantly with wavelength due to resonant collective oscillations of free electrons excited with light (so-called plasmon resonance). Therefore, as well as the absorbed energy, the optical forces and torques will strongly depend on the trapping wavelength [48, 49]. However, the experimental results and theoretical predictions are not in coincidence in the case of optical trapping of larger metal particles ($>$ 170 nm). Models assuming a spherical shape of a NP do not predict its three-dimensional trapping which is, however, observed experimentally by Hansen *et al.* [50, 51] in a tightly focused beam. To explain such surprising behavior we developed a theoretical model based on the coupled dipole method [52], assuming the natural non-spherical morphology of gold NPs [53, 54]. In this paper we use this model to demonstrate complex behavior of plasmonic NPs optically trapped in common optical tweezers with a tightly focused beam. We show here that choosing the proper wavelength of the optical tweezers enables us to modify the trapping conditions, mainly to set the orientation of a non-spherical gold NP nanoparticle with respect to the beam polarization. To prove our theoretical assumptions and model we compare the calculated trapping stiffnesses with published experimental data [51]. Our theoretical results confirm the observed trends reported by other groups. The quantitative coincidence is accessible within one order of magnitude. Another comparison of this theory with our own experimental data, in the case of a beam focused with low numerical aperture (NA) optics, led to better coincidence [55].

2. Theoretical models

The incident tightly focused laser beam (NA = 1.2) was described using the Debye approximation of diffraction of a convergent spherical wave on a circular aperture [37, 56, 57] which is thought to be a highly appropriate case for the description of the strongly focused beam without aberrations [48, 50, 58, 59]. This field distribution was used in all our theoretical models, i.e. in the generalized Lorenz-Mie theory [60, 61] for spherical particles and also in extended the ADDA code [52] based on the discrete-dipole approximation [62] used for spherical but mainly for non-spherical particles. Therefore, we should calculate optical torques and also optical forces [63, 64] acting on a NP of the desired shape. Figure 1 illustrates the trapping ge-

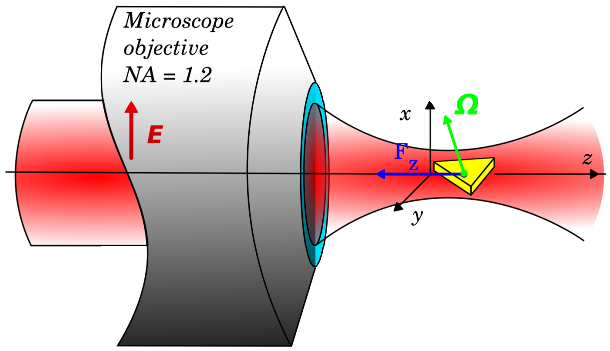

Fig. 1. Trapping geometry of optical tweezers with high NA=1.2. A NP (yellow triangular prism) is trapped laterally on the optical axis and longitudinally slightly behind the beam focus. Its axial position strongly depends on the orientation of the particle with respect to the beam polarization and propagation. The red arrow denotes orientation of the incident electric field $\boldsymbol{E}$ propagating longitudinally along z axis, the blue and green arrow marks the axial optical force F_z and torque $\boldsymbol{\Omega}$ acting on the NP, respectively.

ometry together with the position and orientation of the non-spherical NP near the focus of a tightly focused beam.

3. Theoretical results

3.1. Spherical NP

The majority of theoretical studies or analyses of experimental results consider NPs of spherical shape and therefore the orientation of the beam polarization is not of primary importance for the NP behavior in the optical trap. Figure 2 summarizes the theoretical results related to a single spherical gold NP of six different diameters which is illuminated by high NA optical tweezers at different wavelengths. Spectral dependences of lateral (κ_x, blue curve with circles) and longitudinal (κ_z, red curve with triangles) stiffness of the optical trap reveal which wavelength provides the strongest optical confinement for particular size of gold nanosphere. Accompanying curves for absorption, scattering and extinction cross sections indicate the spectral regions where the absorption and scattering become dominant and how they influence the NP longitudinal confinement. The trap stiffnesses are maximal for trapping wavelengths red-detuned from the plasmon resonance which is determined by the maximal value of the extinction cross-section C_{ext}. This theoretically verifies the experimentally observed concept of plasmon resonance-based optical trapping [37, 48, 49, 65]. However, for a spherical NP larger than 170 nm the scattering is so strong in the investigated spectral region that the considered spherical NP cannot be trapped and is propelled along the beam propagation axis (i.e. the stiffness curves are missing in the last row of Fig. 2).

The results confirm that the light absorption is the principle mechanism forming the scattering force for gold nanospheres with diameters $d < 50$ nm because the scattering cross-section is negligible here. However the light absorption looses its dominance for gold spheres with diameters $d > 50$ nm and at wavelengths longer than 700 nm. Light scattering becomes here the leading source of the scattering force and is responsible for missing optical traps at shorter wavelengths. This trend is also enhanced due to the red shift and broadening of the plasmon resonance peak for larger nanospheres.

#232067 - $15.00 USD Received 8 Jan 2015; revised 27 Feb 2015; accepted 28 Feb 2015; published 23 Mar 2015

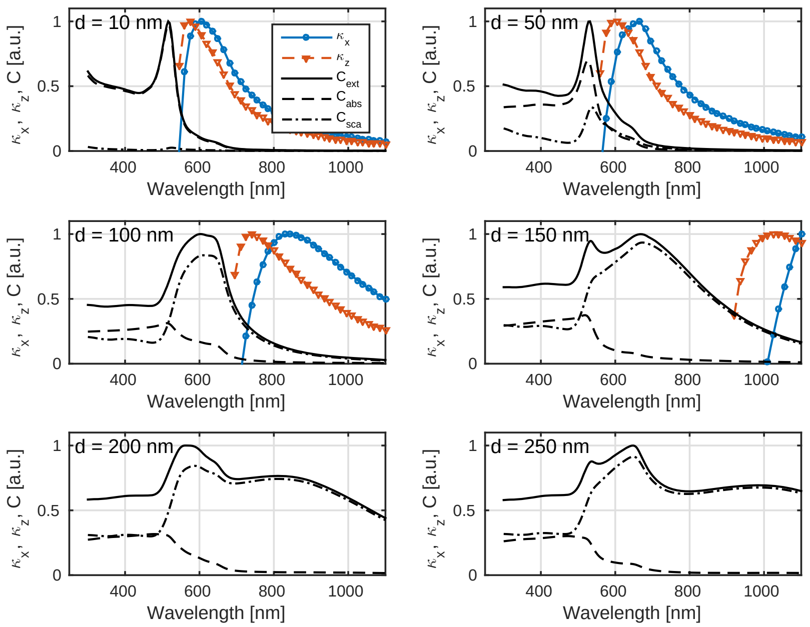

Fig. 2. Absorption, scattering and extinction cross sections calculated for gold nanospheres of various diameter *d* reveal their spectral broadening and red-shift of their maximum with increase of the sphere size. The optical trap stiffness calculated for the same nanospheres placed on the beam axis of a single tightly focused beam of corresponding numerical aperture NA=1.2 is included. The maximum stiffness occurs when the trapping laser wavelength is detuned to the long-wavelength side from the plasmon resonance which is determined by the maximal value of the extinction cross-section C_{ext}. Note that gold nanospheres of diameter larger than 170 nm cannot be optically trapped and therefore the stiffness curves are omitted. The stiffnesses and extinction cross-sections are normalized to their maximum value; absorption and scattering cross-sections are normalized to the maximum of C_{ext} for each particle size.

3.2. Non-spherical NP

The numerical results in Fig. 2 are, however, in contradiction with experimental observations. Hansen *et al.* [51] observed that gold NPs can be stably optically trapped in the same setup even if their diameters are larger than 170 nm. Saija *et al.* [50] have tried to overcome this discrepancy between theory and experiment by suggesting that a steam nanobubble is formed around the trapped nanosphere. However, Messina *et al.* [65] have recently demonstrated that the plasmonic enhanced field plays a crucial role in the optical trapping of gold nanoaggregates with an average size range 20–750 nm. They revealed that plasmon resonances in the fractal structure of the nanoaggregates are responsible for the increased trapping forces and wider trapping range with respect to separated nanospheres. Independently it has been demonstrated [55] that consideration of natural morphology [53, 54] of gold NPs can explain optical confinement of plasmonic NPs using focusing optics with low NA=0.2-0.37. We can thus conclude that nonspherical plasmonic NPs (nanoaggregates, nanorods, prism, etc.) can enhance the optical trapping force when certain plasmon resonances are excited.

Since Hansen *et al.* [51] employed gold NPs from British Biocell, we used the same producer and focused on NPs shapes. Using scanning electron microscopes we observed that shapes shown in Fig. 3 that can be described as decahedrons, icosahedrons, hexagonal and triangular

#232067 - $15.00 USD Received 8 Jan 2015; revised 27 Feb 2015; accepted 28 Feb 2015; published 23 Mar 2015
(C) 2015 OSA 6 Apr 2015 | Vol. 23, No. 7 | DOI:10.1364/OE.23.008179 | OPTICS EXPRESS 8184

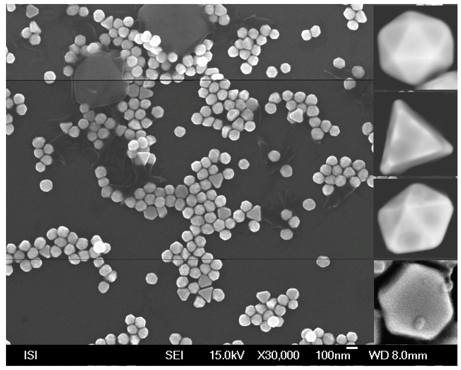

Fig. 3. Gold NPs (diameter 100 nm British Biocell) observed by scanning electron microscopes (JEOL JSM-6700F, FEI Magellan 400). Right-hand column shows detailed images of various particle shapes: icosahedron, triangular prism, decahedron, and hexagonal prism.

prisms. Inspired by the previous studies [66–68], we considered decahedrons and triangular prisms and we set the aspect ratio (the ratio of decahedron half height and the radius of circle circumscribed to its pentagonal base) for gold decahedrons equal to 0.6. In the case of triangular prisms we considered two aspect ratios (the ratio of prism height and the radius of circle circumscribed to triangular base) equal to 0.15 and 0.5. To compare NP of different shapes, we set their volume equal to a sphere of the same volume having so-called equivalent diameter.

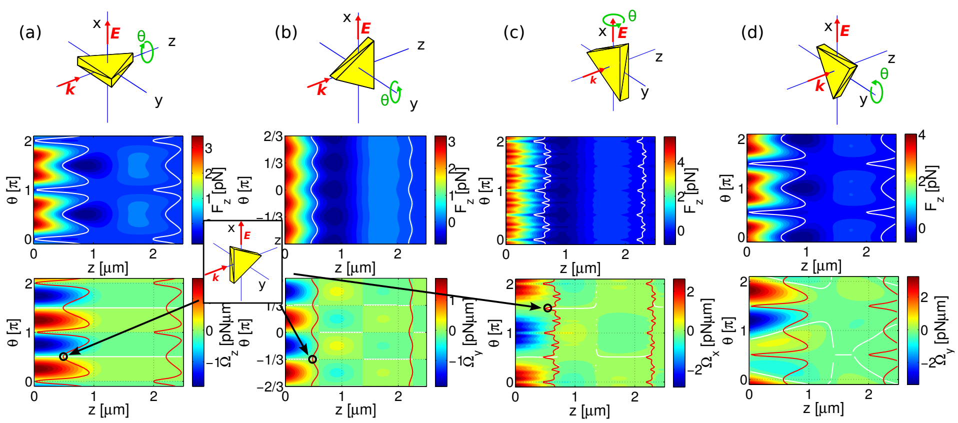

Fig. 4. Stability study of a triangular prism NP of aspect ratio 0.15 and of the same volume as a sphere with the diameter equal to 25 nm illuminated by a focused laser beam (vacuum wavelength $\lambda_{vac} = 1064$ nm, NA 1.2, incident power 1 W) in the non-paraxial description [37, 57]. The first row shows the initial orientation of the studied object ($\theta = 0$) and the positive direction of its rotation. The second row shows the optical force F_z acting on the object in the direction of the beam propagation as the function of the NP longitudinal position ($z = 0$ and $z > 0$ correspond to the position of beam focus and positions behind the beam focus, respectively) and rotation around the denoted axis. The third row shows the optical torque Ω_i acting in direction i of the axis of rotation as the function of the NP longitudinal position and rotation around the denoted axis i. White curves denote equilibrium positions or orientations of the NP. Red curves at the torques maps remind the longitudinal equilibrium position of the NP. The inset in the middle shows the stable NP orientation.

#232067 - $15.00 USD Received 8 Jan 2015; revised 27 Feb 2015; accepted 28 Feb 2015; published 23 Mar 2015

Non-sphericity of gold NPs brings complexity to the studied phenomena because the non-spherical NPs tend to orient with respect to the directions of trapping beam propagation and polarization. Figure 4 shows the results of calculations of optical torques and axial optical force acting on one selected NP of triangular shape. We assumed four different initial NP orientations (see the first row) and NP rotation around different axes so that we could deduce the stable NP orientation and axial position. The second row presents the axial force F_z acting on the NP if it rotates around different axes starting at the particular orientation shown in the first row. The white curves denote the stable positions along z axis for particular angle θ. We can conclude that the studied NP is axially trapped for any orientation of the NP. The bottom row in Fig. 4 deals with the torque acting on the NP for a particular axis of rotation. Equilibrium NP orientations correspond to the white curves where the torque $\Omega_i = 0$ ($i = x, y, z$) and goes from positive to negative values with increasing angle θ. Intersections of these white curves with the red curves (corresponding to the stable axial positions) indicate possible stable trapping orientations and positions of the NP for studied rotation around only one axis. However, the NP can rotate around any axis and thus the stability of such possible stable states must be further proved with respect to these other axes of rotation. For example looking at columns (a) and (b) one comes to the conclusion that the NP stable orientation corresponds to the situation shown in the inset between the columns. Column (c) shows that the NP in this initial orientation tends to rotate to $\theta = \pi/2$ which is the initial orientation studied in the case (b). The column (d) illustrates forces and torques for another possible NP rotation which will gradually develop to the stable orientation shown in the inset between cases (a) and (b).

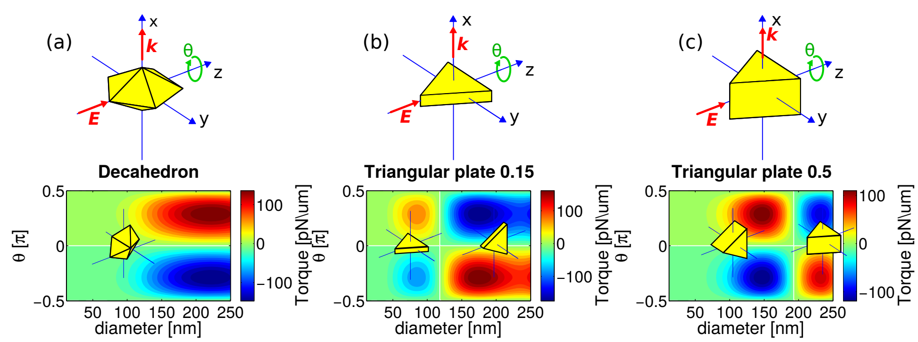

Fig. 5. Stability of a decahedron and triangular prism NP (aspect ratios 0.15 and 0.5) of various sizes illuminated by a focused beam. Sizes of NPs are defined by the volume of a sphere with corresponding diameter. The first row shows the initial orientation of the studied objects ($\theta = 0$) and the direction of rotation. The second row shows the optical torque in the direction of axis of rotation z. (a) Decahedron is stably oriented in parallel with the polarization direction along x axis (i.e. along the vertical axis in the inset). (b) and (c) Smaller triangular prisms are oriented with their base in parallel with the field polarization (vertical axis x in the inset) while base of the larger ones is oriented perpendicularly (along y axis in the inset). The parameters of the beam are the same as in Fig. 4 and the orientation of the axes in the insets are the same as in the first row of Fig. 5.

However for larger NPs or NPs of other shape this stable orientation is not generally valid any more and more complex behavior is presented in Fig. 5. Here we present only torques Ω_z because we found that the stable orientation of the NP is parallel or perpendicular to the beam polarization. Figure 5 demonstrates that the stable orientation of NPs with respect to the polarization of the trapping beam depends on the NPs shape and effective volume. Decahedrons are stably oriented in parallel with the beam polarization for all considered sizes, triangular prism NPs can be stably oriented with their base either in parallel with or perpendicular to

#232067 - $15.00 USD Received 8 Jan 2015; revised 27 Feb 2015; accepted 28 Feb 2015; published 23 Mar 2015

the beam polarization depending on their size. Depending on the aspect ratio of the triangular prisms there exists a particular diameter (in the studied range) where the torque is negligible and thus the NP orientation is not fixed. Note, that this fact can affect the trapping stability and possibly explain observed anomalous behavior of NP of particular size ($d = 154$ nm) in oil objective experiment observed by Hansen, *et al.* [51].

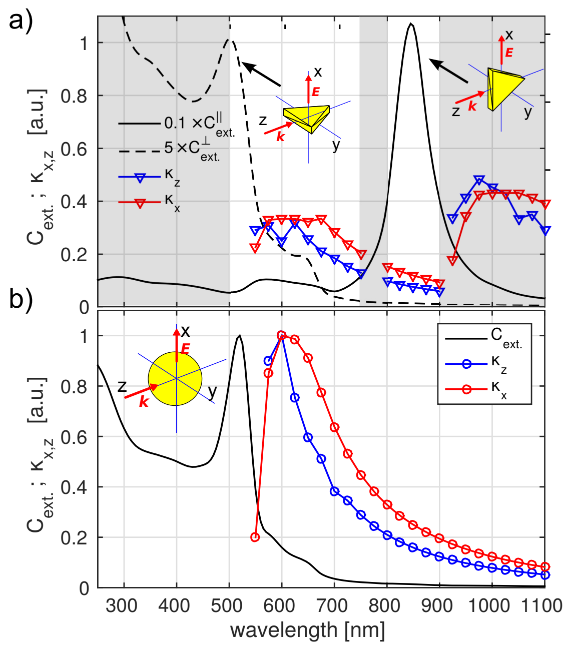

Fig. 6. Extinction cross sections and trap stiffnesses calculated for a) gold triangular prism with effective diameter 25 nm and b) nanosphere of the same volume. Spectral region with gray (white) background corresponds to the stable orientation of the NP in parallel with (perpendicular to) the beam polarization (as illustrated in the insets). Blue and red curves correspond to the longitudinal (κ_z) and lateral (κ_x) stiffness of the optical trap in cases when the NP is trapped in 3D, respectively. The plotted values of the extinction cross-section $C^{\perp}_{\mathrm{ext}}$ and $C^{\parallel}_{\mathrm{ext}}$ correspond to the white and gray region and they are multiplied by 0.1 and 5, respectively, to be both visible in the same plot. All values for the triangular NP at plot a) are plotted relative to the maximal value of quantities obtained for the nanosphere from plot b). Note, that for example the trapping stiffnesses calculated for the triangular prism optically trapped at commonly used wavelength 1064 nm are about 5× larger when compared to the nanosphere.

Recent studies [37,48,69,70] have shown that the gradient force can change its sign depending on the trapping wavelength. Such behavior has been experimentally demonstrated [48,71] by setting the trapping laser wavelength below or above the plasmon resonance wavelength. As we demonstrated in Fig. 2 not only the gradient force but also the scattering force and thus the overall ability to optically trap plasmonic particles depends strongly on the wavelength employed in the optical tweezers. Toussaint *et al.* [49] have recently shown that in the Rayleigh regime the gradient force acting on core-shell nanorods or particles of bi-pyramidal shape can be enhanced when the trapping laser wavelength is slightly red-detuned from the plasmon resonance. Figure 6 demonstrates more complex behavior of a non-spherical NP in the optical tweezers with tunable trapping laser wavelength. We calculated optical forces and

#232067 - $15.00 USD Received 8 Jan 2015; revised 27 Feb 2015; accepted 28 Feb 2015; published 23 Mar 2015

torques acting on the triangular prism (aspect ratio is 0.15) and the nanosphere of the same effective volume placed in optical tweezers with vacuum wavelength varied from 250 to 1100 nm (NA=1.2 and laser power coming through the beam focus equal to 1 W). The values of the refractive index of the NP and medium for considered trapping wavelengths were taken from Palik [72]. For each wavelength we found the stable NP orientation and position in 3D and determined the radial and axial stiffnesses at this position. We compare here the lateral (κ_x) and longitudinal (κ_z) trapping stiffnesses for gold nanosphere and thin triangular prism if they are longitudinally trapped and stably oriented in the laser beam. Stable NP trapping is obtained only at wavelengths where the stiffness points are plotted. According to the stable orientation of the triangular NP, two distinct spectral regions can be identified. The white background denotes NP orientation in parallel with the $y-z$ plane (i.e. perpendicularly to the beam polarization) providing weaker scattering and therefore the NP can be trapped over most of this region. The gray background distinguishes NP orientation in $x-z$ plane (i.e. in parallel with the beam polarization) which provides about two times stronger trap stiffnesses but only in the long-wavelength region. The extinction cross sections and the plotted trap stiffnesses in Fig. 6a are normalized to those calculated for the nanosphere of identical volume shown in Fig. 6b. In fact, we demonstrate here very interesting phenomena, that setting the proper wavelength of the optical tweezers enables us to tune not only the trapping stiffness (as for gold nanospheres) but also the orientation of a non-spherical gold NP with respect to the incident beam polarization.

4. Validation of theoretical model.

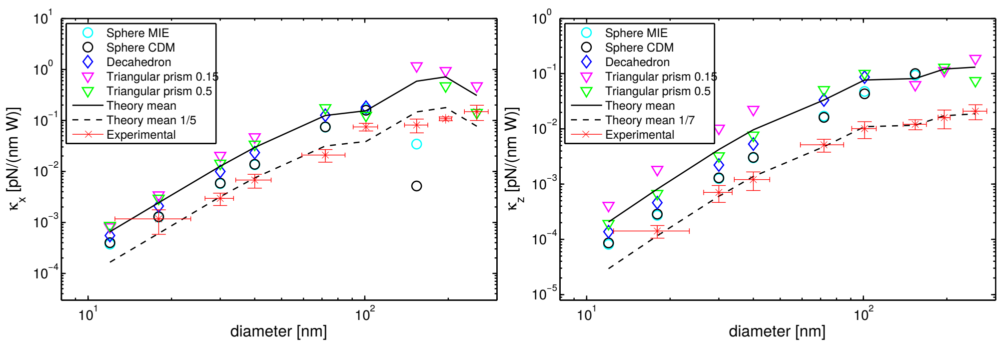

Fig. 7. Comparison of calculated lateral (κ_x) and longitudinal (κ_z) stiffnesses of optically trapped NPs of various effective diameters and shapes with experimental data presented by Hansen *et al.* [51]. We consider spheres, decahedron and triangular prisms with two aspect ratios (height to radius ratio 0.15 and 0.5).

To further validate our assumptions and theoretical model we compared experimental trapping stiffnesses published by Hansen *et al.* [51] with our theoretical results. We considered several shapes of NPs observed in the sample (see Fig. 3) and experimental parameters mentioned in [51] (vacuum wavelength $\lambda_{\text{vac}} = 1064$ nm, numerical aperture of the focusing lens NA = 1.2 and trapping laser power 1W at the sample plane). The results are summarized in Fig. 7 for axial and radial stiffnesses. Note that for each particle shape and size we determined the stable position and orientation in the optical tweezers. The full black curve visualizes the mean value of the trap stiffnesses for all considered NP shapes. Although we considered just a limited number of NP shapes, the scaling of the stiffness with the NP size is very similar to the experimental one. Especially in the case of the longitudinal stiffness κ_z our calculation clearly follows the experimentally observed stiffness behavior for $d > 100$ nm. In the case of a large

#232067 - $15.00 USD Received 8 Jan 2015; revised 27 Feb 2015; accepted 28 Feb 2015; published 23 Mar 2015

triangular NP the theory confirms observed the longitudinal trapping which in contrast does not occur for spherical or decahedron NPs. In order to get precise quantitative overlap of the theoretical and experimental data we had to multiply our theoretical data by a factor of 1/5 and 1/7 for the radial (κ_x) and longitudinal (κ_z) stiffness, respectively. The reason for this quantitative discrepancy is yet unknown but could be caused by differences between the theoretical field description and experimental field distribution because in the case of lower NA we obtained perfect overlap with the theoretical results and measurements [55].

5. Conclusion

We describe complex behavior of plasmonic non-spherical NPs in a tightly focused laser beam. The presented results of numerical calculations indicate that the shape of an optically trapped gold NP strongly determines the stable position and orientation in the optical tweezers for a particular trapping wavelength. We used the coupled-dipole method to determine the stable orientation and position of gold NPs of the following shapes: spheres, decahedrons and triangular prism. Thus the usage of a proper trapping wavelength enables us to set not only the trapping stiffness (as for gold nanospheres) but also the orientation of a non-spherical gold NP. Furthermore, we compared the calculated trapping stiffnesses with the experimental ones presented by Hansen *et al.* [51] and we obtained qualitative agreement with the experimental observations and quantitative agreement within one order of magnitude. We found that relatively large but thin triangular gold prisms can be trapped in 3D even if spheres of the same volume cannot be confined. This brings more clear evidence that the morphology of a plasmonic NP strongly affects the trapping forces. This deepens our understanding of behavior of non-spherical NPs in optical tweezers and promises possible applications as light controlled nanosources of heat or optically trapped nanoprobes with controlled orientation.

Acknowledgments

Authors acknowledge valuable comments of Dr. Stephen Simpson and the SEM characterization carried out by Dr. A. Paták, Dr. Z. Pokorná and Dr. F. Mika. The research was supported by the Czech Science Foundation (project GA14-16195S), the Technology Agency of the Czech Republic (TE01020233) and its infrastructure by the Ministry of Education, Youth and Sports of the Czech Republic (LO1212), Academy of Sciences of the Czech Republic (RVO:68081731) and European Commission (CZ.1.05/2.1.00/01.0017).